Measuring functional renormalization group fixed-point functions for pinned manifolds

A. Alan Middleton[1], Pierre Le Doussal[2], and Kay Jörg Wiese[2]

[1]*Department of Physics, Syracuse University, Syracuse, NY 13244, USA.*
[2]*CNRS-Laboratoire de Physique Théorique de l'Ecole Normale Supérieure, 24 rue Lhomond, 75005 Paris, France.*

(Dated: June 7, 2006)

Exact numerical minimization of interface energies is used to test the functional renormalization group (FRG) analysis for interfaces pinned by quenched disorder. The fixed-point function $R(u)$ (the correlator of the coarse-grained disorder) is computed. In dimensions $D = d + 1$, a linear cusp in $R''(u)$ is confirmed for random bond ($d = 1, 2, 3$), random field ($d = 0, 2, 3$), and periodic ($d = 2, 3$) disorders. The functional shocks that lead to this cusp are seen. Small, but significant, deviations from 1-loop FRG results are compared to 2-loop corrections. The cross-correlation for two copies of disorder is compared with a recent FRG study of chaos.

Systems with quenched (frozen-in) disorder often exhibit glassy phases at low temperature. Standard perturbative methods fail to describe these phases and exact results are limited to 1D and mean field models [1, 2, 3]. It has been quite a challenge to develop field theoretic and renormalization group (RG) methods, which must include both multiple metastable states and spatial fluctuations in finite dimensions, to describe universal properties of these phases. Proposed field theories are unconventional and harder to control than those developed for pure critical systems. An expansion around the mean-field replica symmetry (and ergodicity) broken (RSB) solution, much studied in spin glasses, is very difficult even at the 1-loop level [4]. The functional RG (FRG) was developed for elastic objects pinned by substrate disorder and random fields. This class has numerous physical realizations, including vortex lattices, magnetic systems, and charge density waves [5, 6, 7, 8]. The 1-loop FRG has been extended to describe, e.g., depinning of a driven interface [9], activated dynamics [10], quantum models [11], and sensitivity of configurations to disorder changes ("chaos") [12]. Since the FRG parameterizes the effective action by functions, rather than the few couplings of standard RG, it is better suited to handle an infinite number of marginal parameters at the upper critical dimension (or runaway flows as in correlated fermions [13]).

When applying the FRG to pinned elastic manifolds parameterized by a scalar displacement field $u(x)$, the function in the effective action whose flow is relevant below $d = 4$ is denoted by $R(u)$. Physically, this function represents a coarse graining of the correlator of the pinning potential; it encodes an infinite number of couplings, $R^{(2n)}(0)$, $n = 0 \ldots \infty$. An unusual feature of the theory is that $R''(u)$ can develop a linear cusp around $u = 0$ at finite scale [6]. In the space of non-analytic functions, perturbative control was recovered to one-loop order (i.e., to $O(\epsilon = 4-d)$) and fixed-point functions $R(u)$ obtained for various universality classes [6, 8, 14]. The relations between this cusp singularity, multiple metastable states and shocks in energy landscapes have been vividly described [15]. The FRG agrees with phenomenological models and successfully predicts the roughness exponent ζ of the pinned interface, with the disorder-averaged correlation function $\overline{(u(x) - u(0))^2} \sim x^{2\zeta}$ [16, 17, 18].

Though much has been achieved, it has been questioned [14] whether the FRG can be extended in a systematic loop expansion, i.e., to higher order in ϵ. Dealing with a non-analytic action is very subtle [19], and even 1-loop consistency is not obvious [20]. Recently, a candidate renormalizable field theory for statics [19, 21] (and a distinct one for depinning [22]) was obtained beyond one loop. Crucial to its construction is the property *that the cusp remains linear to higher orders*. If confirmed, the FRG provides a simpler method to attack glass problems where the RSB phenomenology can be avoided.

This paper presents a new level of "smoking gun" tests of the FRG for manifolds, by *directly measuring* the fixed-point function $R(u)$ for three universality classes (Figs. 1-3). This is achieved, as proposed in Ref. [23], by adding to the disorder a parabolic potential (i.e., a mass m) with a variable minimum location v. The resulting sample-dependent free energy $\hat{V}(v)$ defines a renormalized potential whose second cumulant correlator in v space is *the same* $R(v)$ function as defined in the field theory (from the replicated effective ac-

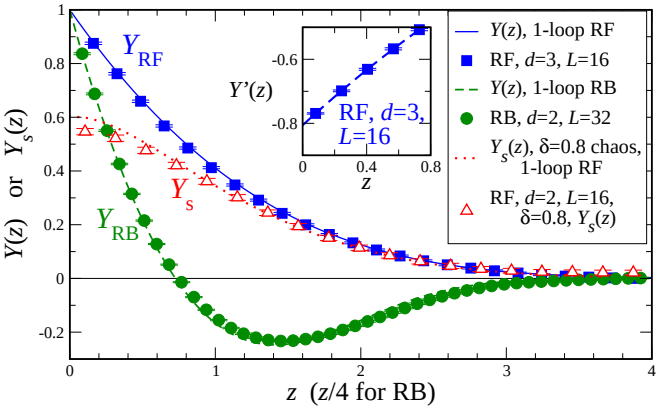

FIG. 1: Filled symbols show numerical results for $Y(z)$, a normalized form of the interface displacement correlator $-R''(u)$ [Eq. (4)], for $D = 2 + 1$ random field (RF) and $D = 3 + 1$ random bond (RB) disorders. These suggest a linear cusp. The inset plots the numerical derivative $Y'(z)$, with intercept $Y'(0) \approx -0.807$ from a quadratic fit (dashed line). Open symbols plot the cross-correlator ratio $Y_s(z) = \Delta_{12}(z)/\Delta_{11}(0)$ between two related copies of RF disorder. It does not exhibit a cusp. The points are for confining wells with width given by $M^2 = 0.02$. Comparisons to 1-loop FRG predictions (curves) are made with no adjustable parameters.

tion - deviations arise only in higher cumulants [23]). This is analogous to measuring the coupling constant and the distribution of total magnetization in pure systems, which underlie phenomenological RG and finite size scaling [24]. As in pure systems, the FRG predictions are universal at coarse grained scales, but require specifying the large scale BCs. The mass provides these conditions and also allows one to control and quantify the zero mode (center of mass) fluctuations, yielding the coupling function $R(u)$. The same procedure allowed an exact calculation [23] of $R(v)$ for the $D = 0 + 1$ theory with RF disorder (Sinai's model).

We numerically compute the FRG zero temperature fixed-point functions using exact ground state configurations. We study interfaces embedded in dimensions $D = d + 1$, $d = 0, 1, 2, 3$, including random bond (RB), random field (RF), and periodic (RP) disorder universality classes. We focus on universal, parameter free functions; treatment of universal amplitudes requires more details and is presented separately [25]. The linear cusp in $\Delta(u) = -R''(u)$ is confirmed in all cases. For periodic disorder, $\Delta(u)$ is consistent with the conjectured parabolic form. For RB and RF disorder, the scaled $\Delta(u)$ are distinct from the 1-loop calculations and are closer to the two-loop results, though the curves exhibit at most a weak dependence on d. The functional shocks responsible for the cusp in $\Delta(u)$ are directly seen. The higher statistics of these shocks are consistent with $d = 0$ Burgers intermittency. Cross-correlation (chaos) fixed points for two related copies of the disorder show a rounding of $\Delta(u)$ that is consistent with recent FRG predictions [12].

The continuum Hamiltonian for an interface $u(x)$ of internal area Ω with elastic constant K, confined in a parabolic well centered at v is

$$\mathcal{H}(v) = \int_\Omega d^d x \left\{ \frac{K}{2} (\nabla u)^2 + \frac{m^2}{2}(u - v)^2 + V[x, u(x)] \right\} \quad (1)$$

where the random potential V has correlations $\overline{V(0, x)V(u, x')} = R_0(u)\delta^{(d)}(x - x')$. The RB universality class describes short ranged $R_0(u)$, the RF class has $R_0(u) \sim -\sigma|u|$ at large u, while the RP class describes periodic correlations, e.g., $R_0(u + 1) = R_0(u)$. The bare correlator $R_0(u)$ becomes $R(u)$ upon coarse graining. Given a UV cutoff scale b, for fixed Ωb^{-d}, and continuous $V(x, u)$, the minimum energy configuration $u(x; v)$ is unique and smoothly varying with v, except for a discrete set of shock positions where $u(x; v)$ jumps between degenerate minima.

For numerics, interfaces $u(x)$ are described by a set I of edge-sharing plaquettes p. Plaquettes are dual to the edges in a regular lattice composed of H layers. Each layer has L^d points, unit cell volume Ω_0, and periodic BCs. Each point is connected to points in the layer above by κ bonds, so that an interface I has κL^d plaquettes [25]. The energy $\mathcal{H}_{\rm latt}$ of I, confined by a well of strength M centered at v, is

$$\mathcal{H}_{\rm latt}(v) \;=\; \sum_{p \in I} \left\{ \frac{M^2}{2}[u(p) - v]^2 + U(p) \right\}, \quad (2)$$

where $u(p)$ is the layer index for plaquette p and $U(p)$ is the disorder potential. Long-wavelength elasticity arises from combinatorial effects [16]. For RB disorder, $U(p)$ is a Gaussian variable $h(p)$ with zero mean and variance $\sigma_0^2 = 1$, while for RF disorder $U(p)$ is the sum of $h(p)$ along a path of edges connecting p to the bottom layer. RP disorder with period P is constructed by stacking H/P identical RB samples of thickness P. Given $U(p)$, v, and M, the ground state $I_{\rm gs}$ is found using a program that accommodates all lattices, dimensionalities, and disorder types. The new version of the core max-flow algorithm [16] in our code has been directly tested against standard libraries [26] and earlier energy minimization calculations [16, 17, 18]. The height H is always large enough that the finite size effects are controlled only by L and M. Lattice discreteness is evident at high values of M, so we choose $M < 0.2$. Continuum and discrete models are then related by equating energies $\mathcal{H}_{\rm latt}$ and $\mathcal{H}$, displacements $u(p)$ and $u(x)$, interface areas $\Omega_0 \kappa b^d L^d = \Omega$, well strengths $m^2 = M^2(\Omega_0 b^d)^{-1}$, and disorder strengths $\sigma = \frac{\kappa\sigma_0}{2\Omega_0 b^d}$. The effective elastic constant K was also measured [25].

We computed the discrete force-force correlation [23]:

$$\Delta_{\rm latt}(v) = M^4(\kappa L^d)\overline{[v' + v - u_0(v' + v)][v' - u_0(v')]}, \quad (3)$$

where the mean position $u_0(v) = (\kappa L^d)^{-1} \sum_{p \in I_{\rm gs}} u(p)$. The averaging (overline) is for $N > 10^4$ samples with $0 \le v' < P$ for RP disorder; RF and RP samples are self-averaging over v' (we slide v' over more than 10^5 times the interface width while computing minima in a window of thickness $H \approx 20$ centered at v'). The plots we present have 1σ error bars computed using direct resampling of the data and are thus expected to overlap the large sample number limit with a probability of 68%. To check our procedure, we confirm that $\int_0^\infty du\, \Delta_{\rm latt}(u)$ is consistent within errors with the value σ_0 for RF disorder and with the value 0 for RB and RP disorders.

The FRG predicts that, for large volumes Ω/b^d, the rescaled correlator $\tilde{\Delta}(z)$, defined by $\Delta(u) = m^{\epsilon - 4\zeta}\tilde{\Delta}(um^\zeta)$, converges as $m \to 0$ to the FRG fixed-point function $\tilde{\Delta}^*(z)$, which depends only on d and disorder. Using Eq. (3), convergence of $M^{4\zeta-\epsilon}\Delta_{\rm latt}(zM^{-\zeta})$ was evident for $L > 16$ ($L > 8$ in $d = 3$) and $M < 0.2$, choosing [16] $\zeta = 2/3, 0.44, 0.22$ for $d = 1, 2, 3$ RB disorder and $\zeta = (4 - d)/3$ for RF disorder. The interface widths grow slowly ($\zeta = 0$) for RP disorder. As the FP functions still contain an amplitude and a scale, we introduce the normalized function $Y(z)$,

$$\Delta(u) = \Delta(0)Y(u/\xi), \quad (4)$$

so that $Y(0) \equiv 1$ and with scale ξ chosen according to disorder type: for the RP model, $\xi = P$, for RF disorder, ξ is set so that $\int_0^\infty dz\, Y(z) = 1$, and for RB disorder, $\int_0^\infty dz\, Y^2(z) = 1$. This function is predicted to be universal with a dependence in d, $Y(z; d)$, that can be computed to second order in $\epsilon := 4 - d$ [19, 21]

$$Y(z; d) = Y_1(z) + \epsilon Y_2(z) + O(\epsilon^2), \quad (5)$$

with $Y_1(z)$ the 1-loop estimate [6, 8, 14]. Computation of K is required to fix universal information not retained in $Y(z)$, e.g., the amplitude $\Delta(0)$ for RF disorder [25].

We plot illustrative examples of $Y(z)$ in Fig. 1. In all cases, an apparently linear cusp is found for $Y(z)$ (with finite intercepts for fits to $Y'(z)$). The normalized functions are remarkably close to 1-loop predictions, with no adjustable parameter. We now turn to a systematic analysis of these functions, their deviation from 1-loop results, and related data.

We start with RF disorder. The FRG predictions for the functions $Y_1(z)$ and $Y_2(z)$ in (5) are obtained from linearizing the $O(\epsilon^2)$ relation [21] $z = \frac{\sqrt{Y-1-\ln Y-\frac{\epsilon}{3}F(y)}}{\int_0^1 dy\sqrt{y-1-\ln y-\frac{\epsilon}{3}F(y)}}$, where $F(y) = 2y - 1 + \frac{y\ln y}{1-y} - \frac{1}{2}\ln y + \mathrm{Li}_2(1-y)$. Plots of the differences $Y(z) - Y_1(z)$ between the numerical result and the 1-loop prediction [6], for several sizes and masses in $D = 2{+}1$ and $D = 3{+}1$, are shown in Fig. 2. There are small, but statistically significant, systematic deviations from $Y_1(z)$. The sign of the expected corrections linear in ϵ, $Y_2(z)$, agrees with numerics. This function changes sign at $z_c = 1.668\ldots$, near the observed location. The magnitude of $\epsilon Y_2(z)$, setting $\epsilon = 1$, is nearly consistent with numerics for all d. We include $0+1$ numerical results (compatible with Refs. [23, 27]) for comparison. Points for $D = 2+1, 3+1$ are both close to $D = 0+1$ results. Our computed slopes at the origin, $-Y'(0) = 0.815(7)$ (3+1) and $-Y'(0) = 0.811(6)$ (2+1), are to be compared with the FRG value $0.7753\ldots + (0.0328\ldots)\epsilon$ and the $d = 0$ [23] value $0.8109\ldots$. The near equality of the $d = 0$ curve and $Y_2(z)$ appears to be a coincidence. Although more work is needed to resolve the differences (e.g., $d = 0$ from $d = 2, 3$) the trend of the FRG results is encouraging.

For RB disorder, $R(u)$ is expected to decay (so $\Delta(u)$ has a zero). Fixing ξ as stated sets a non-universal scale. The differences $Y(z) - Y_1(z)$ are plotted in Fig. 2: we again find small but significant deviations from the 1-loop prediction, with at most a weak dependence on d (within error bars). The $O(\epsilon^2)$ expansion in this case is found from series and numerical solutions [21]. The resulting $Y_2(z)$ again agrees well in sign and shape with the data, with a magnitude given by $\epsilon \approx 1$. We have constructed 2-loop interpolations which agree with the data in all d [25]. The situation resembles that for RF disorder, even though deviations have the opposite sign.

Results for the function $Y(z)$ for RP disorder are shown in Fig. 3 for $d = 3$; similar results hold for $d = 2$. The 1- and 2-loop FRGs predict [8, 21] a parabolic form, $\Delta(u) = \Delta(0)(1 - 6u(1-u))$, as do the $d = 0$ and the large-d cases (with a single shock as $m \to 0$ [15] and many small independent shocks per period [20], respectively). Counting of derivatives in the FRG equation has also indicated that the parabolic form holds for any finite d. The parabolic form is consistent with our results as $m \to 0$.

The use of a harmonic well allows one to define and study the shocks in the force landscape. As v increases, sections of the manifold have degenerate minima at positions v_s and the polarization jumps forward by $\int d^dx\,[u(x; v_s^+) - u(x; v_s^-)]$. These are shocks in a functional (scalar for $d = 0$) decaying Burgers equation [23], with the renormalized force $v - u(v)$ corresponding to velocity and m^{-1} corresponding to time in Burgers turbulence. Examples of these discontinuities in the renormalized force are shown in the inset of Fig. 4. We have seen shocks merge as m decreases [25]. The moments of the renormalized force are $S_n(v - v') = \overline{(v - v' - u(v) - u(v'))^n}$. A linear cusp in S_2 is confirmed by our study of $\Delta(v)$. A prediction of the FRG in $d > 0$ [23] is that $S_3(v - v') \sim (v - v')$ at small $v - v'$, in accord with exact results for $d = 0$. Linearity of all S_n, $n \geq 2$ is a hallmark of intermittency in $d = 0$ Burgers turbulence. Our data show linearity of S_3 (Kolmogorov scaling) and S_4 in $v - v'$ for cases studied. This indicates that shocks do not cluster beyond simple statistical fluctuations.

When the pinning potential is perturbed, correlations between the original and perturbed samples remain for RF disorder and are described by a new chaos FRG fixed point [12]. We test this prediction using related disorders $U_1(p)$ and $U_2(p) = [U_1(p) + \delta \cdot W(p)]/\sqrt{1+\delta^2}$, where the perturbation $W(p)$ is a mean-zero univariate Gaussian and δ is the perturbation strength. We measured the cross correlator $\Delta_{12}(v - v') = \kappa L^d M^4 \overline{(v - u_{0,1}(v))(v' - u_{0,2}(v'))}$. We check the sum rule $\int_0^\infty du\,\Delta_{12}(u) = \sigma/\sqrt{1+\delta^2}$ and normalize via $Y_s(z) = \Delta_{12}(\xi z)/\Delta_{11}(0)$. We find (Fig. 1) that $Y_s(z)$

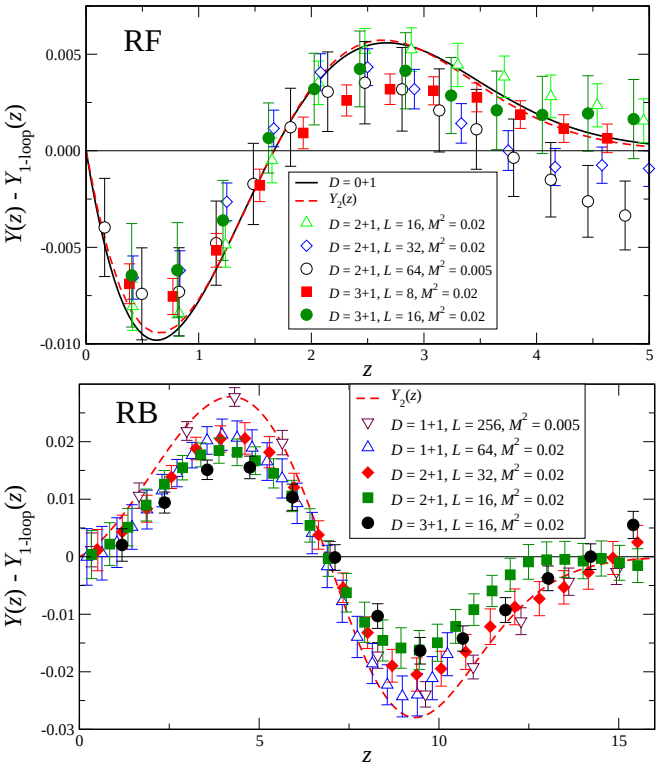

FIG. 2: The difference between the normalized correlator $Y(z)$ and the 1-loop prediction $Y_1(z)$ for RF disorder in $D = (1, 2) + 1$ and RB disorder in $D = (1, 2, 3) + 1$. The dashed lines are the linear 2-loop correction $Y_2(z) = \frac{dY(z)}{d\epsilon}|_{\epsilon=0}$ of Eq. (5). For each disorder class, the data are close to each other and to the $d = 0$ and $\epsilon = 1$ linear two-loop estimates, but are distinct from the 1-loop result.

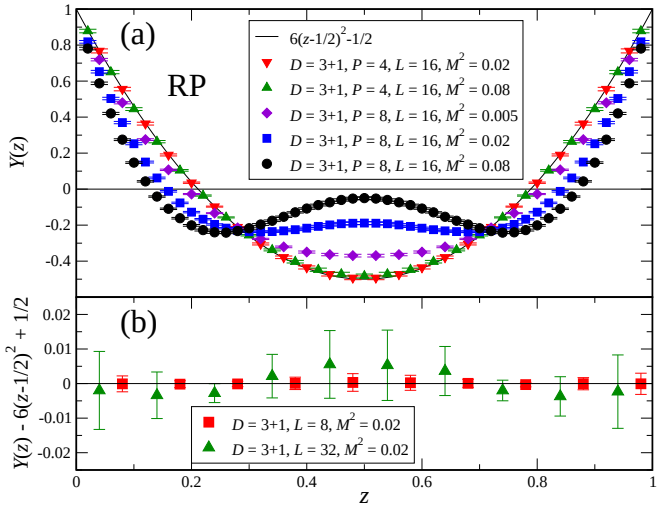

FIG. 3: (a) Plots of the normalized pinning force correlator $Y(z)$ for RP disorder in $d = 3$. For these values of m, the period $P = 4$ points have mostly converged to the parabolic RP fixed-point function, while the $P = 8$ curves are still crossing over from the RB to the RP universality class. (b) Residuals relative to the parabolic shape vanish, within error bars, for larger sizes and $P = 4$.

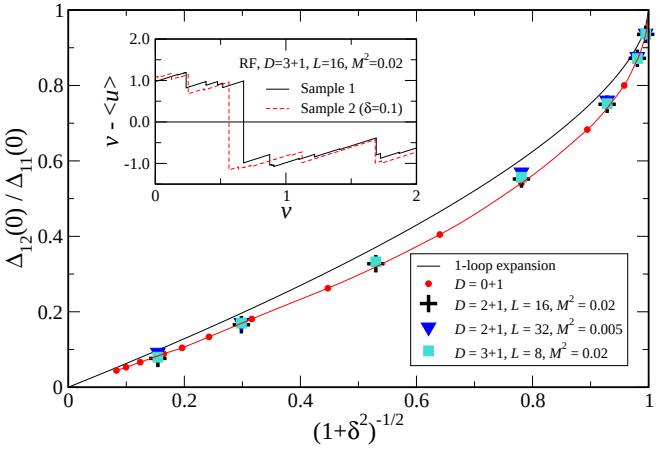

FIG. 4: A plot of the normalized cross-correlator $\frac{\Delta_{12}(0)}{\Delta_{11}(0)}$, computed for RF disorder in $d = 2, 3$, showing the sensitivity to disorder of magnitude δ, compared to the 1-loop prediction and to numerical $D = 0 + 1$ computations (error bars not shown; 1σ errors are about $1/2$ of symbol size). Inset: the renormalized pinning forces $v - u_0(v)$ for a sample (solid line) and a $\delta = 0.1$ perturbed sample (dashed line) in a typical sample; cross-correlations of such data give the main plot.

is rounded, as predicted [12]. The computed $Y_s(0)$ is near the 1-loop prediction (see Fig. 4).

Our numerical calculations confirm the main features of the FRG approach to the glassy system of pinned interfaces, especially the shape of $R''(u)$ and its linear cusp, for a variety of disorders and dimensionalities. FRG computations to 2-loop order significantly improve upon the 1-loop results. The functional shocks found are consistent with expectations; their statistics merit further study.

The authors thank the KITP and the Aspen Center for Physics for their hospitality. We acknowledge support from NSF Grants 0109164 and 0219292 (AAM) and ANR program 05-BLAN-0099-01 (PLD and KW).

[1] D.A. Huse, C. L. Henley and D.S. Fisher, Phys. Rev. Lett. **55**, 2924 (1985).
[2] K. Johansson, Commun. Math. Phys. **209**, 437 (2000).
[3] M. Mezard and G. Parisi, J. Phys. I **1**, 809 (1991).
[4] C. de Dominicis, *et al*, in A.P. Young, editor, *Spin glasses and Random Fields*, World Scientific, Singapore, 1997.
[5] T. Nattermann, and C. Belanger, *Ibid*.
[6] D.S. Fisher, Phys. Rev. Lett. **56** 1964 (1986) and Phys. Rev. B **31**, 7233 (1985).
[7] G. Blatter, *et al*, Rev. Mod. Phys. **66**, 1125 (1994); T. Nattermann and S. Scheidl, Advances in Physics **49** (2000) 607.
[8] T. Giamarchi and P. Le Doussal, Phys. Rev. B **52**, 1242 (1995).
[9] O. Narayan and D.S. Fisher, Phys. Rev. B **48**, 7030 (1993). Nattermann, *et al*, J. Phys. II (France) **2**, 1483 (1992).
[10] P. Chauve, T. Giamarchi, P. Le Doussal, Phys. Rev. B **62**, 6241 (2000).
[11] L. Balents, Europhys. Lett. **24**, 489 (1993).
[12] P. Le Doussal, cond-mat/0505679.
[13] C.J. Halboth and W. Metzner, Phys. Rev. B **61**, 7364 (2000).
[14] L. Balents and D.S. Fisher, Phys. Rev. B **48**, 5949 (1993).
[15] L. Balents and J.P. Bouchaud and M. Mézard, J. Phys. I (France) **6**, 1007 (1996).
[16] A.A. Middleton, Phys. Rev. E **52**, R3337 (1995); D. McNamara, A.A. Middleton and C. Zeng, Phys. Rev. B **60**, 10062 (1999).
[17] see e.g. M.J. Alava, P.M. Duxbury, C. Moukarzel and H. Rieger in *Phase transitions and critical phenomena*, Ed. C. Domb and J. L. Lebowitz, Academic Press, San Diego, **18**, 141 (2001).
[18] J.D. Noh and H. Rieger, Phys. Rev. Lett. **87**, 176102 (2001).
[19] P. Chauve, P. Le Doussal and K. Wiese, Phys. Rev. Lett. **86**, 1785 (2001).
[20] L. Balents and P. Le Doussal, Annals of Physics, **315**, 213 (2005); P. Chauve and P. Le Doussal, Phys. Rev. E **64**, 051102 (2001); S. Scheidl, Y. Dincer cond-mat/0006048.
[21] P. Le Doussal, K.J. Wiese and P. Chauve, Phys.Rev. E **69**, 026112 (2004); P. Le Doussal, K. J. Wiese, Phys. Rev. E **72**, 035101(R) (2005), Phys. Rev. Lett. **89** 125702 (2002).
[22] P. Le Doussal, K.J. Wiese and P. Chauve, Phys. Rev. B **66**, 174201 (2002).
[23] P. Le Doussal, cond-mat/0605490 and in preparation.
[24] K. Binder, Z. Physik B **43**, 119 (1982); E. Brezin and J. Zinn-Justin, J. Nucl. Phys. B **257**, 867 (1985); T.W. Burkhardt, B. Derrida, Phys. Rev. B **32**, 7273 (1985).
[25] P. Le Doussal, A. Middleton, K. J. Wiese, to be published, and a longer work, in preparation.
[26] A. V. Goldberg, Optimization Library, available at http://www.avglab.com/andrew/.
[27] O. Duemmer, to be published.